Transactions of NAMP 24, (2026) 119-134

Transactions of
The Nigerian Association of
Mathematical Physics
Journal homepage: https://nampjournals.org.ng

THEORETICAL ANALYSIS OF ION TRANSPORT IN CASSAVA STARCH-POLYVINYLPYRROLIDONE NANOCOMPOSITE POLYMER ELECTROLYTES FOR LITHIUM-ION BATTERY PERFORMANCE

IYAMU C.O.[1]

[1] *Department of Physics, Nasarawa State University, Keffi, Nasarawa State.*

ARTICLE INFO

Article history:
Received xxxxx
Revised xxxxx
Accepted xxxxx
Available online xxxxx

Keywords:
Nanocomposite polymer electrolyte,
Cassava starch,
Polyvinylpyrrolidone,
Lithium salt,
Ion transport,
Ion-transport models.

ABSTRACT

Due to the growing demand for eco-friendly and sustainable energy storage systems, this study presents an analysis of ion transport in cassava starch (CS)- polyvinylpyrrolidone (PVP) nanocomposite polymer electrolytes for improved lithium-ion battery (LIB) applications. In this study, five electrolyte samples were produced using the direct-heat solution casting method. The data obtained from these samples were analyzed using SEM micrographs, and theoretical models including ionic conductivity equation, Nernst-Einstein equation, Fick's law of diffusion, and Faraday's law of electrolysis. The results showed that Sample 3, which contained equal amounts of CS and PVP, exhibited a smooth surface with minimal cracks and the highest ionic conductivity $(1.74\ x\ 10^{-3}\ S/cm)$*, diffusion coefficient* $(3.34\ x\ 10^{-9}\ cm^2/s)$*, diffusion flux* $(2.31\ x\ 10^{-4}\ mol/m^2.s)$*, and electric charge* $(3.94\ x\ 10^{-3}\ C/s)$*. The high ion transport properties observed in Sample 3 indicate excellent homogeneity between the components of the electrolyte film, making it ideal for enhanced lithium-ion battery applications.*

1 INTRODUCTION

The growing demand for energy storage systems, particularly LIB, has necessitated increased investigation into ion transport in nanocomposite polymer electrolytes. In polymer electrolyte, lithium salts serve as charge carriers by supplying mobile lithium ions (Li^+) [1]. Lithium salt dissociates within the electrolyte system, allowing Li^+ to migrate through the polymer matrix and conduct electric charge [2]. The motion of Li^+ and the rate at which they move inside the polymer matrix determine the electrolyte's ability to conduct electric charge. Thus, polymers and nanoparticles play a significant role in enhancing Li^+ transport [3].

*Corresponding author: IYAMU C.O
E-mail address: caesariyamu71@gmail.com
https://doi.org/10.60787/tnamp.v24.672

According to Zhang [4], polymers act as the host matrix for ion transport because they contain functional group chains, such as ether (-C-O-C-) groups in synthetic polymers or hydroxyl (-OH-) groups in biopolymers. These functional groups provide coordination sites that enable Li^+ to hop along the polymer backbone, thereby enhancing ionic mobility [5,6]. In addition, nanoparticles modify the polymer matrix through interfacial interactions with the polymer chains [7]. Their nanoscale size, typically between 5 and 100 nm, results in a high surface-area-to-volume ratio, which increases the amorphous content of the polymer matrix and creates additional pathways for ion transport [8].

The pathways created by polymers and nanoparticles enable Li^+ to move more rapidly toward the cathode to maintain charge balance, while electrons travel toward the anode through the external circuit, generating electric current. These simultaneous ionic and electronic movements contribute directly to the material's macroscopic electrochemical performance, commonly observed during the charging and discharging cycles of batteries [9].

The charging-discharging cycles give LIBs longer lifespans and faster charging capabilities compared to traditional batteries [10]. As a result, LIBs are widely used in various applications ranging from small electronic devices such as smart phones and laptops to large-scale systems such as electric vehicles and renewable energy storage devices [11].

Ion transport properties, which are related to impedance values, are experimentally determined using Electrochemical Impedance Spectroscopy (EIS). These impedance values are further analysed using theoretical models, including ionic conductivity model [12], the Nernst-Einstein model [13], Fick's law of diffusion [14] and Faraday's law of electrolysis [15].

In this study, nanocomposite polymer electrolytes consist of CS biopolymer and PVP synthetic polymer in varying mass proportions, while lithium acetate dihydrate salt, titanium dioxide nanoparticles, glycerol plasticizer and borax crosslinker are maintain at fixed proportions. The variation of CS and PVP compositions is intended to determine the formulation that produces the best ion-transport performance, while simultaneously assessing the viability of CS as a sustainable alternative material.

In energy storage systems, biopolymer materials such as cellulose and starch derivatives are being investigated as alternatives to synthetic polymers because of the environment challenges associated with synthetic polymers. Synthetic polymers are plastic-based materials that are often toxic and non-biodegradable nature [16], whereas [17] emphasized that biodegradable materials are inexpensive, abundant, less toxic, and environmentally friendly.

Research on biopolymers used either wholly or partially to replace synthetic polymers in nanocomposite polymer electrolytes is relatively recent compared to the numerous studies on polymer electrolytes that utilize only synthetic polymers [18]. However, findings from [19] on the effect of lithium salts on the properties of cassava starch solid biopolymer electrolytes showed that the highest ionic conductivity was achieved using lithium sulphate salt. Similarly, another study by [20] on the influence of various concentrations of lithium triflate on the electrochemical properties of cassava starch biopolymer electrolytes revealed that the highest ionic conductivity value was obtained at a salt concentration of 0.17 mol.

As a result of the important role played by polymers in ion transport and the subsequent enhancement of electrochemical properties, this study investigates the performance of ion-transport mechanisms using a composite blend of CS and PVP polymers for LIBs.

2 THEORETICAL MODEL FOR ION TRASPORT MECHANISMS

The theoretical model for ion transport used in this study is based on the frequency-dependent response theory proposed by [21]. This theory assumes that ion transport in an electrolyte depends on the frequency response of the applied signal. Information on the frequency response of the applied signal in the nanocomposite polymer films was obtained from EIS. This technique was used to analyse ion transport properties, including ionic conductivity, diffusion coefficient, diffusion flux and electric charge. These parameters were evaluated using the ionic conductivity model, the Nernst-Einstein equation, Fick's law of diffusion, and Faraday's law of electrolysis, respectively.

a. Ionic Conductivity Equation

The ionic conductivity values of Samples 1-5 were calculated using Equation (1).

$$\sigma = \frac{L}{R_b \,.\, A} \tag{1}$$

Where:

$\sigma =$ ionic conductivity of the samples (S/cm)
$L =$ thickness of the samples (cm)
$R_b =$ Bulk resistance (Ω) of the samples and corresponds to the point on the real impedance axis (Z_{real}) of the Nyquist plot where the curve begins to rise steadily.
$A =$ Area of the samples (cm^2)

Since the samples are circular, the area of the samples is obtained as follows:

$$A = \pi(d/2) \tag{2}$$

where $d =$ diameter of the samples (cm)

b. Nernst-Einstein Model

Nernst-Einstein model is used to derive the diffusion coefficient (D) by relating it with ionic conductivity [22]. The diffusion coefficient values of Samples 1-5 were calculated using Equation (3).

Nernst-Einstein equation [23] is expressed as:

$$\sigma = \frac{\mathrm{n}Z^2e^2D}{K_BT} \tag{3}$$

Making the diffusion coefficient (D) the subject of the formula;

$$D = \frac{K_BT\sigma}{\mathrm{n}Z^2e^2} \tag{4}$$

Where:

σ = ionic conductivity of the samples (S/cm)
$n =$ number density of charge carrier $(LiCH_3COO.2H_2O)$ $(ions/cm^3)$
$z =$ charge number of Li^+ $(z = 1\ for\ Li^+)$
$e =$ elementary charge of Li^+ $(1.602x10^{-19}C)$
$D =$ diffusion coefficient of the samples (cm^2/s)
$K_B =$ Boltzmann constant $(1.38x10^{-23}J/K)$
$T =$ absolute temperature in Kelvin (K)

The number density of charge carrier ($LiCH_3COO.2H_2O$), (n) was calculated using Equations $(4) - (8)$.

$$n = C_{salt}\, x\, N_A \quad (5)$$

$$C_{salt} = \frac{M_{salt}}{V_{dry\ film.}} \quad (6)$$

$$M_{salt} = \frac{m_{salt}}{mm_{salt}} \quad (7)$$

thus, $$n = \left(\frac{m_{salt}}{mm_{salt} x\, V_{dry\ film.}}\right) x\, N_A \quad (8)$$

$N_A =$ Avogadro's number ($6.022x10^{23} mol^{-1}$)

C_{salt} = concentration of charge carrier ($LiCH_3COO.2H_2O$)

M_{salt} = Moles of charge carrier ($LiCH_3COO.2H_2O$)

m_{salt} = mass of lithium salt in the samples

mm_{salt} = molar mass of charge carrier ($LiCH_3COO.2H_2O$) = ($102.02 g/mol$)

$mm_{salt} = Li: (1x\ 6.94 g/mol) + C\ (2\ x\ 12.01 g/mol) + H\ (7\ x\ 1.008 g/mool) + O\ (4\ x\ 16 g/mol) = 102.02\ g/mol$

$V_{dry\ film.}$ = volume of the samples

$$V_{dry\ film.} = \pi\, d^2 L \quad (9)$$

Where:

$d =$ diameter of the samples

$L =$ thickness of the samples

c. Fick's Law of Diffusion

Fick's law of diffusion is used to derive the diffusion flux of a sample by relating it with their diffusion coefficient. Fick's law of diffusion states that the diffusion flux is proportional to the negative gradient of concentration. It can also be defined as the number of moles of ions passing through a unit area per unit time [14]. The diffusion flux values of Samples 1-5 were calculated using Equation (10).

The Fick's first law of diffusion [14] is expressed as:

$$J = -D\frac{dC}{dx} \quad (10)$$

$$but\ \frac{dC}{dX} \approx \frac{C}{L}$$

Therefore, $$J = -D\frac{C}{L} \quad (11)$$

Where:

$J =$ diffusion flux of the samples ($mol/m^2.s$)

$D =$ diffusion coefficient of the samples (m^2/s)

$\frac{dC}{dX}$ = concentration gradient ($mol\ /\ m^4$)

$C =$ concentration of lithium salt ($mol\ /\ m^3$)

$L =$ thickness of the samples (m)

d. Faraday's Law of electrolysis

Faraday's law of electrolysis is used to derive the electric charge of a sample by relating it with their diffusion flux. Faraday's first law of electrolysis states that the amount of substance deposited at an electrode during electrolysis is directly proportional to the quantity of electric charge passed through the electrolyte [15]. The electric charge values of Samples 1-5 were calculated using Equations $(12) - (15)$.

The Faraday's first law of electrolysis [15] is expressed as:

$$n = \frac{Q}{ZF} \quad (12)$$

Making the electric charge (Q), the subject of the formula

$$Q = n\,.Z.F \quad (13)$$

but $n = JAt$ (14)

thus $Q = J.A.t.Z.F$ (15)

Where:

$n =$ moles of Li^+ $(mole)$ of the samples

$Q =$ electric charge $(Coulombs)$ of the samples

$J =$ diffusion flux of the samples

$A =$ area of the samples

$t = 1\ sec.$ This is the theoretical time for diffusion-based ion transport in a polymer electrolyte [15].

$Z =$ valence of $Li^+ = +1$

$F =$ Faraday's constant = $96,485\ C/mol$

3 MATERIALS AND METHOD

3.1 Materials

The materials used in this work consist of lithium acetate dihydrate $(LiOOCCH_3.2H_2O)$ (99%), polyvinylpyrrolidone (PVP) (98%), cassava starch powder (95%), titanium dioxide (TiO_2(99%), borax (98%), glycerol (98%), and deionized water (99.9%). Cassava starch powder was locally prepared, while $LiOOCCH_3.2H_2O$, PVP, TiO_2, borax, glycerol and deionized water were purchased through a vendor at African University of Science and Technology, Galadima, FCT-Abuja.

3.2 Preparation of Cassava Starch Powder

Cassava starch powder was prepared based on [19] procedures. The procedures involved washing and peeling off the skin of a cassava tubers. The peeled tubers were then disintegrated by grinding using industrial grinding processor. The grinded tubers were then placed in deionized water, stirred for 15mins, and filtered through muslin cloth. The filtered liquid was left to settle down for 12 hrs., to allow it to precipitate. The precipitated starch was obtained after removing water left on top of it. The precipitated cassava starch was then washed three times with deionized water and dried in an oven for 24 hrs. at 50^0C. The dried precipitated cassava starch was then grinded using household electric grinding machine to obtain cassava starch powder.

3.3 Preparation of Nanocomposite Polymer Electrolyte Films

The nanocomposite polymer electrolyte films were prepared using direct heating solution casting method as illustrated by [24]. The nanocomposite polymer electrolyte materials composition is presented on Table 1.

Table 1: Compositions of Cassava Starch-Polyvinylpyrrolidone Nanocomposite Polymer Electrolytes

Sample	CS (g)	PVP (g)	Glycerol (ml)	Borax (g)	Titanium Dioxide (g)	Lithium Acetate dihydrate (g)
S1	0	5	2	0.3	0.15	0.5
S2	1.5	3.5	2	0.3	0.15	0.5

S3	2.5	2.5	2	0.3	0.15	0.5
S4	3.5	1.5	2	0.3	0.15	0.5
S5	5	0	2	0.3	0.15	0.5

Based on the above material compositions, five CS-PVP nanocomposite polymer electrolyte samples were prepared using the direct-heat solution casting method. As shown in Figure 1, CS and PVP solutions were prepared using 15-50mL of deionized water. The solution was then heated at 60^0C for 30 minutes and stirred using a magnetic stirrer at 750rpm. After 30 minutes, glycerol was added and mixed for another 10minutes. Subsequently, borax and TiO_2 were added and further mixed for another additional 10 minutes. Finally, lithium acetate dihydrate was added and mixed with the solution for another 20 minutes. At end of the 20 minutes, the solution was cast onto three Teflon sheets and dry at room temperature for 48hrs. The dried films were then peeled off using a razor blade and used for the experiments.

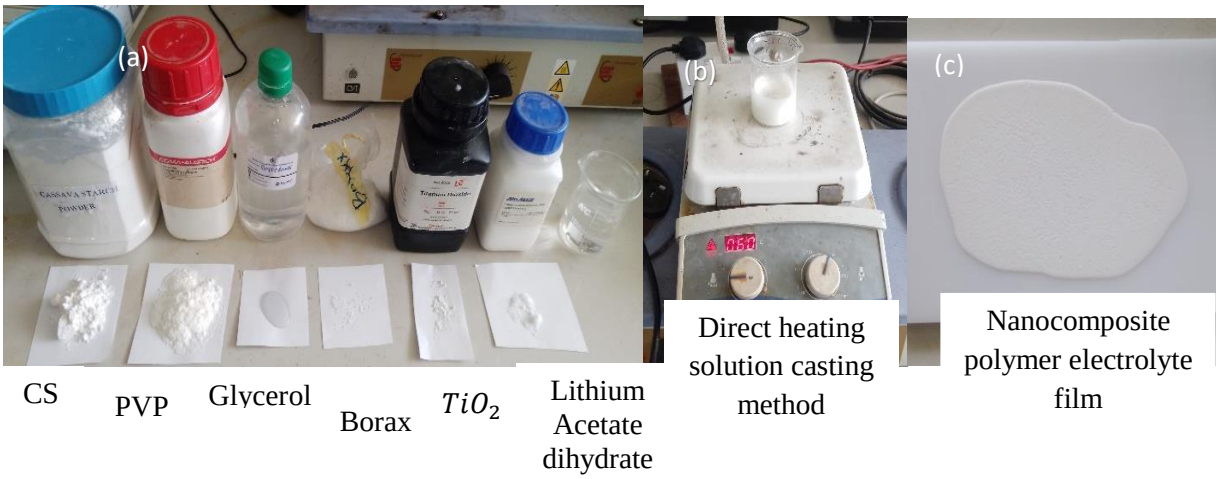

Figure 1: **(a)** Materials of CS-PVP nanocomposite polymer electrolytes, **(b)** The prepared polymer electrolyte solutions, based on the sample compositions, were heated on a hot-plate magnetic stirrer. In addition, a magnetic stirrer bar was placed inside the solution to ensure uniform mixing, **(c)** nanocomposite polymer electrolytes placed on a Teflon sheet, and allow to dry at room temperature.

3.4 Scanning Electron Microscopy Method

Scanning Electron Microscopy was used to collect data on SEM surface morphology images of nanocomposite polymer electrolyte films. The instrument used consist of Tescan Vega 3 SEM to capture an image at an accelerating voltage of 15kV at field of view of $745\mu m$ and magnification size of 500x, to enable detailed surface analysis. SEM imagery data was analyzed using visual method to check out for surface defects such as roughness, cracks, voids, and nanoparticle agglomeration. These defects reveal the miscibility levels of the nanocomposite polymer electrolyte film preparations, and this level is likely to affect ion transport and mechanical strength [25].

3.5 Electrochemical Impedance Spectroscopy Method

Electrochemical Impedance Spectroscopy was used to obtain data on impedance (Nyquist) plot of nanocomposite polymer electrolyte films. Data were collected using Gamry Instruments Reference 600 (Potentiostat/Galvanostat/ZRA). The electrolyte films were sandwiched between two-coin cells, which is a stainless-steel blocking electrode. Impedance data were collected over a frequency

range of 1Hz to 1MHz with an applied AC amplitude of 10mV at room temperature. The complex impedance spectra were analysed using Gamry software to generate Impedance (Nyquist) plot (real vs. imaginary impedance). EIS data was analyzed using electrical properties models consisting of ionic conductivity equation [6], Nernst-Einstein model [23], Fick's law of diffusion [14], and Faraday's law of electrolysis [15].

RESULTS AND DISCUSSION

4.1 Surface Morphology of Nanocomposite Polymer Electrolytes

The SEM images showing the topography of Samples 1-5 at a magnification of 500x are presented in Figure 2.

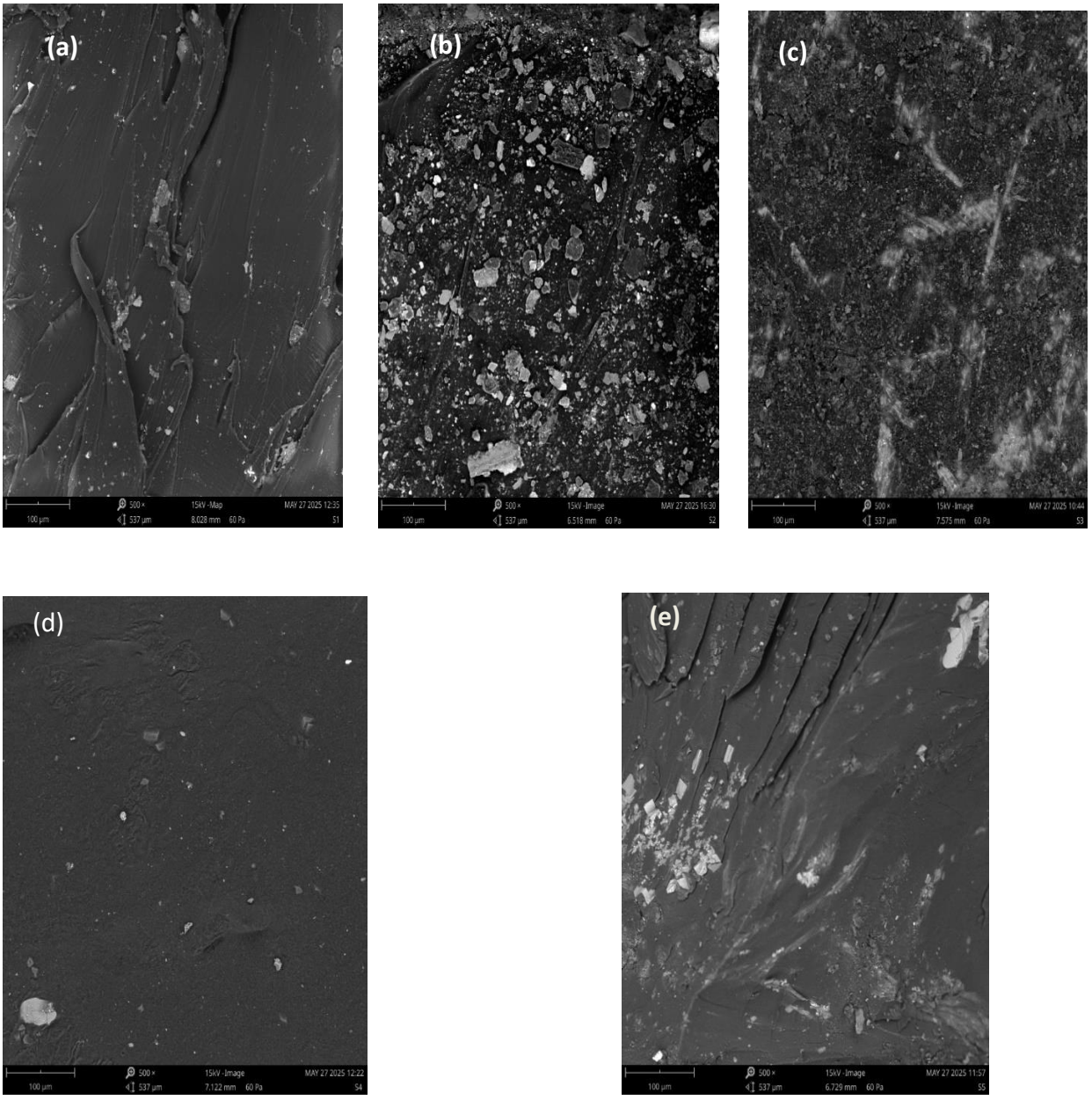

Figure 2: SEM micrographs showing the topography of **(a)** Sample 1 (0g CS, 5g PVP),

(b) Sample 2 (1.5g CS, 3.5g PVP), **(c)** Sample 3 (2.5g CS, 2.5g PVP), **(d)** Sample 4 (3.5g CS, 1.5g PVP), **(e)** Sample 1 (5g CS, 0g PVP). Apart from CS and PVP mass ratio, all the samples contain fixed amount of 2ml glycerol, 0.3g borax, 0.15g titanium oxide and 0.5g lithium acetate dihydrate. The topography of the samples was scan using an accelerating voltage of 15kV, and at field of view of 745µm and magnification size of 500X, to enable detailed surface analysis.

The SEM results revealed distinct microstructural features influenced by the varying ratios of CS and PVP. Samples 3 and 4 exhibited the smoothest surfaces with minimal cracks, indicating better mixing and compatibility of the material components. This was followed by Samples 1, 5, and 2, respectively.

The smoother and more uniform surfaces observed in Samples 3 and 4 suggest that the CS and PVP polymers formed a more homogenous matrix at these compositions. This improved compatibility between the polymers may have enhanced the distribution of the components within the electrolyte film, resulting in fewer structural defects such as cracks and surface irregularities. A homogenous microstructure indicates that the polymer chains are well integrated, forming a compact structure that can support stable material properties.

In contrast, the relatively rougher surfaces observed in Samples 1, 5, and 2 indicate less uniform structural formation within the polymer matrix. The presence of more visible irregularities and cracks suggests weaker interaction between CS and PVP at these compositions, which may lead to uneven component distribution during film formation process.

The improved surface uniformity observed in Samples 3 and 4 may also facilitate better ion transport within the polymer electrolyte. In polymer electrolyte systems, ion migration typically occurs through the amorphous regions of the polymer matrix where polymer chain mobility is higher. Therefore, a smoother and more homogenous microstructure can create more continuous pathways for Li^+ movement, which may enhance ionic conductivity.

These findings agree with the reports of [26, 27, 17], who reported that smooth surfaces with uniform particle distribution and minimal voids enhance ion transport and ionic conductivity in polymer electrolyte systems. Overall, the SEM observations indicate that the intermediate CS-PVP compositions in Samples 3 and 4 promote better structural compatibility within the polymer electrolyte matrix, which may support improved ion transport and electrolyte performance.

4.2 Ion Transport Analysis of Nanocomposite Polymer Electrolytes

4.2.1 Ionic Conductivity Model

The ionic conductivity of Sample 1-5 was examined using Nyquist plot and ionic conductivity equation as presented in Figure 3(a-e) and Table 2.

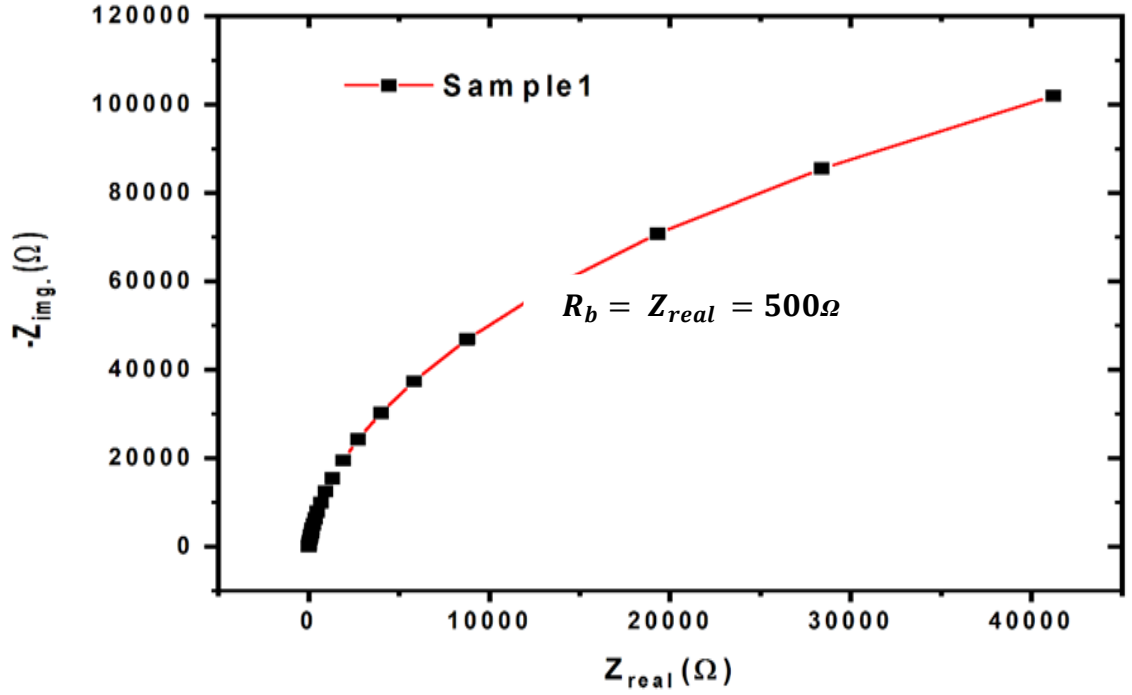

Figure 3a: Electrochemical impedance Nyquist Plot of Sample 1 (0g CS, 1.5g PVP) recorded using a frequency range of 1Hz to 1MHz with an applied AC amplitude of 10mV at room temperature. The bulk resistance of the sample, $R_b = 500\Omega$ from the plot is used to analyse the ionic conductivity.

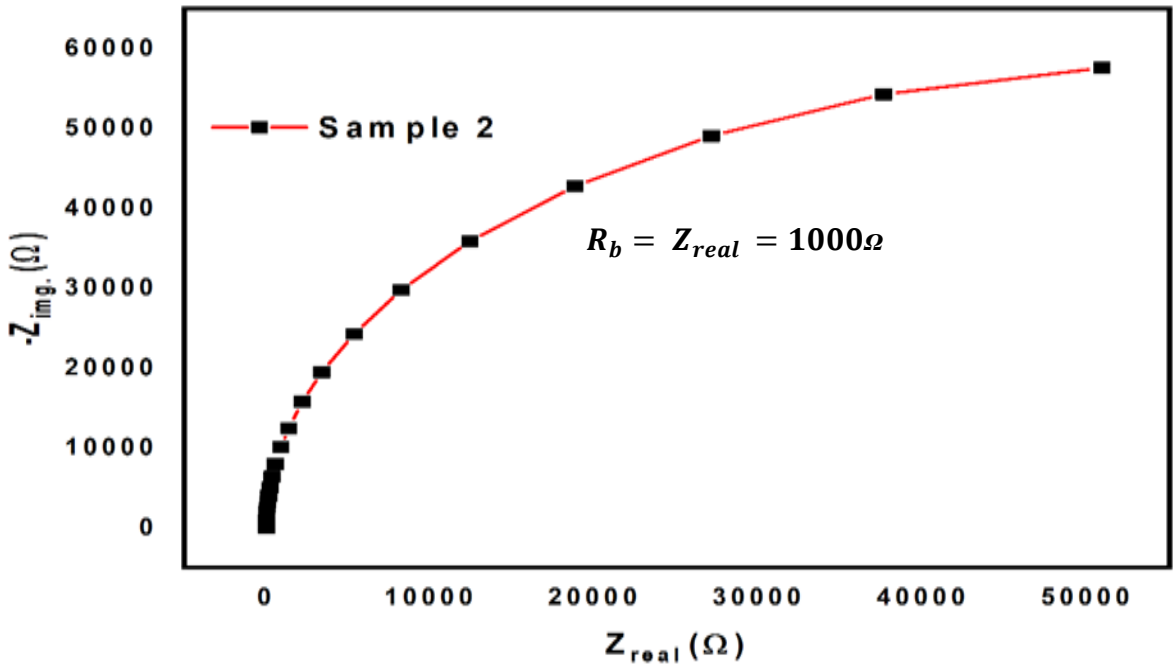

Figure 3b: Electrochemical impedance Nyquist Plot of Sample 2 (1.5g CS, 3.5g PVP) recorded using a frequency range of 1Hz to 1MHz with an applied AC amplitude of 10mV at room temperature. The bulk resistance of the sample, $R_b = 1000\Omega$ from the plot is used to analyse the ionic conductivity.

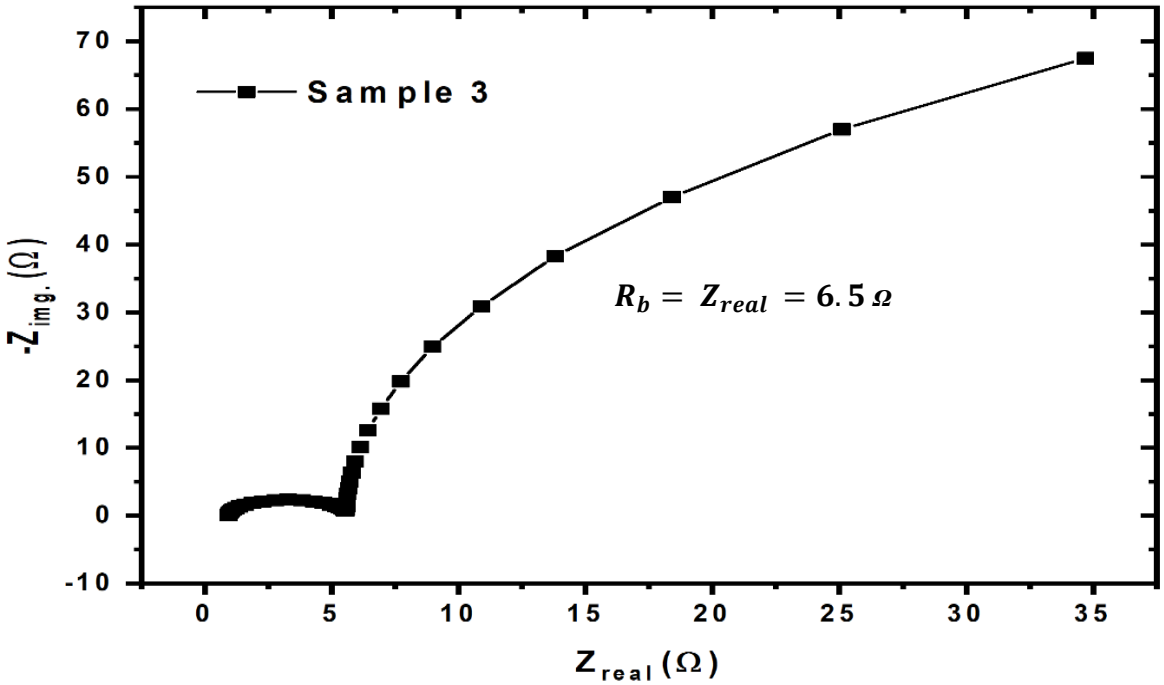

Figure 3c: Electrochemical impedance Nyquist Plot of Sample 3 (2.5g CS, 2.5g PVP) recorded using a frequency range of 1Hz to 1MHz with an applied AC amplitude of 10mV at room temperature. The bulk resistance of the sample, $R_b = 6.5\,\Omega$ from the plot is used to analyse the ionic conductivity.

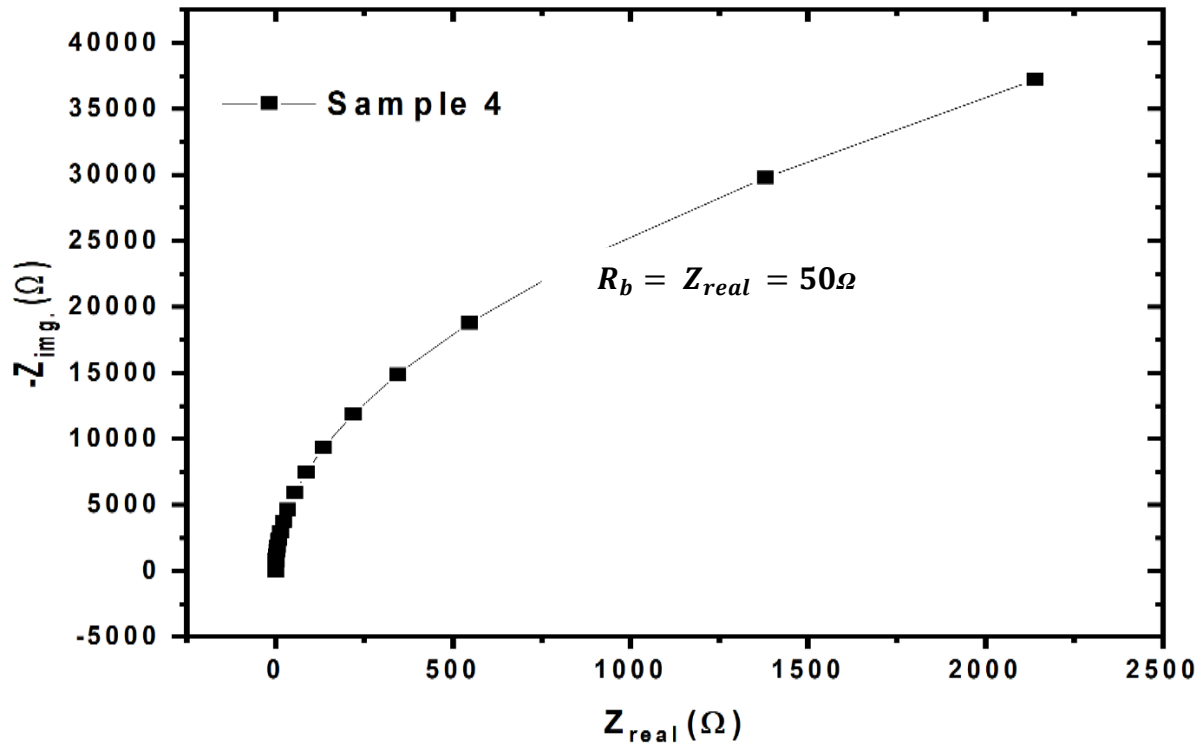

Figure 3d: Electrochemical impedance Nyquist Plot of Sample 4 (3.5g CS, 1.5g PVP) recorded using a frequency range of 1Hz to 1MHz with an applied AC amplitude of 10mV at room temperature. The bulk resistance of the sample, $R_b = 50\Omega$ from the plot is used to analyse the ionic conductivity.

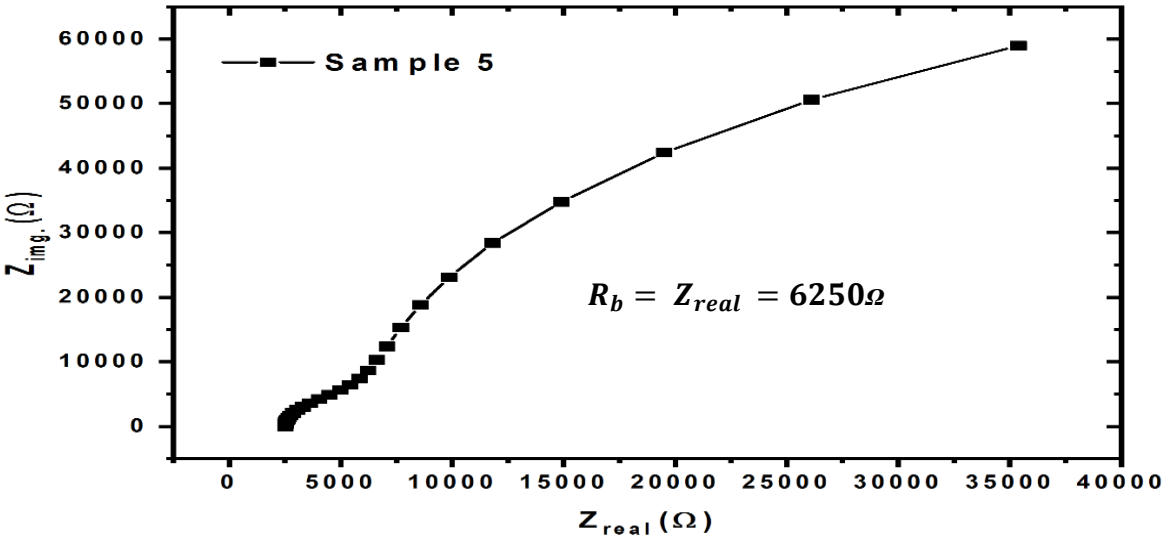

Figure 3e: Electrochemical impedance Nyquist Plot of Sample 5 (5g CS, 0g PVP) recorded using a frequency range of $1Hz$ to $1MHz$ with an applied AC amplitude of 10mV at room temperature. The bulk resistance of the sample, $R_b = 6250\Omega$ from the plot is used to analyse the ionic conductivity.

Table 2: Ionic conductivity of Samples 1-5 with varying CS:PVP ratios, using bulk resistance (R_b) of each sample.

Sample	$R_b\ (\Omega)$	Thickness, L (cm)	Diameter, D (cm)	Area, A (cm^2)	Ionic Conductivity, σ (S/cm)
1 $(0g\ CS, 5g\ PVP)$	500	0.02	1.5	1.77	$2.26\ x\ 10^{-5}$
2 $(1.5g\ CS, 3.5g\ PVP)$	1000	0.02	1.5	1.77	$1.13\ x\ 10^{-5}$
3 $(2.5g\ CS, 2.5g\ PVP)$	6.5	0.02	1.5	1.77	$1.74\ x\ 10^{-3}$
4 $(3.5g\ CS, 1.5g\ PVP)$	50	0.02	1.5	1.77	$2.26\ x\ 10^{-4}$
5 $(5g\ CS, 0g\ PVP)$	6250	0.02	1.5	1.77	$1.81\ x\ 10^{-6}$

The ionic conductivity results of Samples 1-5 as presented in Table 2, revealed a compositional trend that may be attributed to the varying blend ratios of CS and PVP. The ionic conductivities of all samples fall within the typical range reported for polymer electrolytes, $10^{-6} - 10^{\cdot -3} S/cm$ [22], however, Sample 3 exhibited the highest ionic conductivity of $1.74x10^{-3}\ S/cm$. This suggests that the balanced proportion of CS and PVP may have created an optimal polymer network that enhanced ion transport within the electrolyte matrix. These results agree with several reported studies including [9, 28, 19, 29]. However, it is in contrast with [30] who reported a lower ionic conductivity of 10^{-11}s/cm for corn starch-lanthanum nitrate systems.

Ionic conductivity in polymer electrolytes is influenced by the concentration of mobile charge carriers and the segmental motion of the polymer chains. At the intermediate CS-PVP composition observed in Sample 3, interactions between the hydroxyl groups of CS and the carbonyl groups of PVP may have improved salt dissociation, thereby increasing the number of free Li^+ available for conduction. The blending of the polymers may also reduce crystallinity and increase the amorphous phase, where ion transport mainly occurs. Furthermore, the balanced composition may have increased the free volume within the polymer matrix, creating additional pathways for ion migration.

4.2.2 Nernst-Einstein Model

The diffusion coefficients of sample 1-5, was analysed using Nernst-Einstein model, with the results summarized in Table 3.

Table 3: Diffusion coefficients of Samples 1-5 with varying CS:PVP ratios, using ionic conductivity (σ) of each sample.

Sample	σ (S/cm)	K_B (J/K)	Temp. (K)	Number Density, n $(ionscm^3)$	Valence z	Elementary Charge, C	Diffusion Coefficient D (cm^2/s)
1	$2.26x10^{-5}$	$1.38x10^{-23}$	298	$8.337x10^{22}$	1	$1.602x10^{-19}$	$4.34x10^{-11}$
2	$1.13x10^{-5}$	$1.38x10^{-23}$	298	$8.337x10^{22}$	1	$1.602x10^{-19}$	$2.17x10^{-11}$
3	$1.74x10^{-3}$	$1.38x10^{-23}$	298	$8.337x10^{22}$	1	$1.602x10^{-19}$	$3.34x10^{-9}$
4	$2.26x10^{-4}$	$1.38x10^{-23}$	298	$8.337x10^{22}$	1	$1.602x10^{-19}$	$4.34x10^{-10}$
5	$1.81x10^{-6}$	$1.38x10^{-23}$	298	$8.337x10^{22}$	1	$1.602x10^{-19}$	$3.48x10^{-12}$

The diffusion coefficient results of Samples 1-5 as presented in Table 3, revealed a trend that may be influenced by the varying CS and PVP in the polymer electrolyte matrix. Among the samples, Sample 3 exhibited the highest diffusion coefficient of $3.34x10^{-9}\ cm^2/s$. This result is consistent with the ionic conductivity findings, where Sample 3 also recorded the highest ionic conductivity. The higher diffusion coefficient observed for Sample 3 suggests that Li^+ diffuse more easily through the polymer matrix, resulting in improved ionic conductivity.

The balanced composition of CS and PVP in Sample 3 may have produced a polymer network with improved segmental mobility and increased amorphous regions. These amorphous regions provide free volume and flexible pathways that facilitate ion migration through the electrolyte, while the improved chain flexibility enhances the diffusion mechanism of Li^+ between coordination sites within the polymer matrix.

4.2.3 Fick's Law of Diffusion

The diffusion fluxes of Sample 1-5 were analysed using Fick's law of diffusion, with the results summarized in Table 4.

Table 4: Diffusion fluxes of Samples 1-5 with varying CS:PVP ratios, using diffusion coefficient (D) of each sample.

Sample	Diffusion Coefficient, D (cm^2/s)	Concentration, c $(mol./m^3)$	Thickness, L (m)	Diffusion Flux, J $(mol./m^2.s)$
1	$4.34x10^{-11}$	$1.38x10^5$	0.0002	$2.995x10^{-6}$
2	$2.17x10^{-11}$	$1.38x10^5$	0.0002	$1.50x10^{-6}$
3	$3.34x10^{-9}$	$1.38x10^5$	0.0002	$2.31x10^{-4}$
4	$4.34x10^{-10}$	$1.38x10^5$	0.0002	$2.99x10^{-5}$

5	$3.48x10^{-12}$	$1.38x10^{5}$	0.0002	$2.40x10^{-7}$

The diffusion flux results of Samples 1-5, presented in Table 4, revealed a trend that may be influenced by the varying proportion of CS and PVP in the blend. Among the samples, Sample 3 demonstrated the highest diffusion flux of $2.31x10^{-4}\ mol/m^2s$, suggesting that this composition promotes more efficient Li^+ transport. This observation aligns closely with the trends observed in both the ionic conductivity and diffusion coefficient results, indicating a strong correction between diffusion flux and overall ion mobility in the polymer electrolyte.

The higher diffusion flux observed in Sample 3 may be attributed to its balanced CS:PVP ratio, which likely creates optimal polymer network structure. This network accelerates the flows of Li^+ migration through a unit areas of the surface per unit time because of its concentration gradient, thereby maximizing ion transport and enhancing electrochemical performance of the nanocomposite polymer electrolyte.

4.2.4 Faraday's Law of Electrolysis

The electric charges of Sample 1-5, was analysed using Faraday's law of electrolysis as presented in Table 5.

Table 5: Electric charges of Samples 1-5 with varying CS:PVP ratios, using diffusion flux (J) of each sample.

Sample	Diffusion Flux, J $(mol./m^2.s)$	Area (m^2)	Model Time (s)	Valence, z	Faraday's Constant (F)	Electric Charge, Q (C)
1	$2.995x10^{-6}$	0.000177	1	1	96,485	$5.11x10^{-5}$
2	$1.50x10^{-6}$	0.000177	1	1	96,485	$2.56x10^{-5}$
3	$2.31x10^{-4}$	0.000177	1	1	96,485	$3.94x10^{-3}$
4	$2.99x10^{-5}$	0.000177	1	1	96,485	$5.11x10^{-4}$
5	$2.40x10^{-7}$	0.000177	1	1	96,485	$4.1x10^{-6}$

The electric charge results of Samples 1-5, shown in Table 5 revealed that Sample 3 exhibited the highest electric charge of $3.94x10^{-3}C/s$, indicating that it allows the greatest flow of electric charge through the polymer electrolyte. It further indicates that the quantity of charges transported by ions per unit time, suggest that Sample 3 possesses the highest density of mobile Li^+ and the least resistance to their movement. This aligns with the trends observed in ionic conductivity, diffusion coefficient, and diffusion flux, confirming that the optimal CS: PVP blend enhances ion transport efficiency.

CONCLUSION

The Li^+ transport in CS- PVP nanocomposite polymer electrolytes were analysed using ion transport theoretical models based on EIS measurements. The findings reveal that Sample 3, with an equal blend proportion of CS and PVP, exhibited the fastest ion transport and superior electrochemical properties, with an ionic conductivity of $1.74x10^{-3}$ S/cm, a diffusion coefficient of $3.34x10^{-9}cm^2/s$, a diffusion flux of $2.31x10^{-4}mol/m^2.s$, and an electric charge of $3.94x10^{-3}C/s$.

The results demonstrated that the variation in CS: PVP composition significantly influences ion transport in the nanocomposite polymer electrolytes, where higher ionic conductivity corresponds to higher diffusion coefficient, diffusion flux, and electric charge, indicating enhanced mobility and transport of Li^+ within the polymer matrix. This enhanced Li^+ transport may also be attributed to the smoother and more homogenous surface morphology observed in the SEM micrograph of Sample 3.

REFERENCES

[1] Brooks, D. J., Merinov, B. V., Goddard, W. A., Kozinsky, B., & Mailoa, J. (2018). Atomistic descriptive of ionic diffusion in PEO-LiTFSI: Effect of temperature, molecular weight and ionic concentration. *Macromolecules*, 51, 21, 8987-8995. https://doi.org/10.1021/acs.macromol.8b01753

[2] Xu, K. (2004). Nonaqueous liquid electrolytes for lithium-based rechargeable batteries. *Chemical Reviews*, 104, 10, 4303-4417.https://doi.org/10.1021/cr030203g

[3] Griffiths, D. J. (2008). *Introduction to elementary particles* (2nd ed.). Wiley. https://doi.org/10.1002/9783527618460

[4] Zhang, S. S. (2006). A review on electrolyte additives for lithium-ion batteries. *Journal of Power Sources*, 162, 1379-1394. https://doi.org/10.1016/j.jpowsour.2006.07.074

[5] Zixuan, W., Jialong, F., & Xin, G. (2025). Conduction of lithium ions in polymer electrolytes. *Solid State Ionics*, Volume 424, June 2025, 116858. https://doi.org/10.1016/j.ssi.2025.116858

[6] Yan, G. (2020). Mechanical behaviour of solid electrolyte materials for lithium-ion battery. *Energy and Environmental Science.* https://www.researchgate.net/publication/358575303

[7] Kumar, N., Sahu, D. K., & Mahipal, Y. K. (2023). Effect of TiO_2 on ion transport properties and dielectric relaxation of sodium ion-conducting novel PEO/PAN-blended solid polymer electrolyte. *Journal of Materials Research*, 38(19) https://doi.org/10.1557/s43578-023-00984-0

[8] Li, J., Zeng, Y., & Zhang, X. (2016). Metal oxide nanostructures for energy storage and conversion: A review. *Journal of Materials Chemistry A,* 4, 2, 526-546. https://doi.org/10.1039/c5tao7720a

[9] Chu, H. J. (2023). Potential composite solid-state electrolyte for lithium-ion batteries (Master's thesis). University of California, United States of America. https://escholarship.org/content/qt0hw617b8/qt0hw617b8_noSplash_dc5331a24959dc767c8d7c75d3cfda6b.pdf

[10] Azemtsop, M. T. (2013). Progress into lithium-ion battery research. *Journal of Chemical Research*. May-June 1-9. https://doi.org/10.1177/17475198231183349

[11] Kittel, C. (2005). *Introduction to solid state physics* (8th ed.). Wiley. http://metal.elte.hu/~groma/Anyagtudomany/kittel.pdf

[12] Macdonald, J. R., & Barsoukov, E. (2005). *Impedance Spectroscopy: Theory, experiment, and applications*. John Wiley & Sons, Inc., Hoboken. https://doi.org/10.1002/0471716243

[13] Armand, M., & Tarascon, J. M. (2008). Building better batteries. *Nature*, 451, 7159, 652-7. https://doi.org/10.1038/451652a

[14] Fong, K. D., Self, J., McCloskey, B. D., & Persson, K. A. (2021). Ion correlations and their impact on transport in polymer-based electrolytes. *Macromolecules*, 54, 6, 2575-2591. https://doi.org/10.1021/acs.macromol.0c02545

[15] Bard, A. J., & Faulkner, L. R. (2001). *Electrochemical methods: Fundamentals and applications* (2nd ed.). Wiley. https://www.wiley.com/en-us/Electrochemical+Methods%A+Fundamentals+and+Applications%2C+2nd+Edition-p-9780471043720

[16] Wang, X., Zhai, H., Qie, B., Cheng, Q., Li, A., Borovilas, J., Xu, B., Shi, C., Jin, T., Liao, X., Li, Y., He, X., Du, S., Fu, Y., Dontigny, M., Zaghib, K., & Yang, Y. (2019). Rechargeable solid-state lithium metal batteries with vertically aligned ceramic nanoparticle polymer composite electrolyte. *Nano Energy*, *60*, *205-212*. https://doi.org/10.1016/j.nanoen.2019.03.051

[17] Raihan, R., Fairuzdzah, A. L., Asiah, M. N., & AbMalik, M. A. (2022). The compatibility of jackfruit seed starch and polyvinyl alcohol blend as biopolymer electrolyte host. *Malaysian Journal of Analytical Sciences*, 26, 4, 829-837. https://mjas.analis.com.my/mjas/v26_n4/pdf/Raihan_26_4_13.pdf

[18] Patra, N., Ramesh, P., Donthu, V., & Ahmad, A. (2024). Biopolymer-based composites for sustainable energy storage: Recent developments and future outlook. *Journal of Materials Sciences: Materials in Engineering*, 19,1, 34. https://doi.org/10.1186/s40712-024-00181-9

[19] Arrieta, A. A., Calabokis, O. P., & Mendoza, J. M. (2023). Effect of lithium salts on the properties of cassava starch on solid biopolymer electrolytes. *Polymers*, 15 (20), 1-3. https://doi.org/10.3390/polym15204150

[20] Arrieta, A. A., Calabokis, O. P., & Vanegas, C. (2024). Influence of lithium triflate salt concentration on structural, thermal, electrochemical, and ionic conductivity properties of cassava state solid biopolymer electrolytes. *International Journal of Molecular Sciences*, 25, 15, 8450, https://doi.org/10.3390/ijms25158450

[21] Lasia, A. (2014). *Electrochemical Impedance Spectroscopy and its Applications*. Springer. https://doi.org/10.1007/978-1-4614-8933-7

[22] Wang, W., & Alexandridis, P. (2016). Composite polymer electrolytes: Nanoparticlesa affect structure and properties. *Polymers 2016*, 8(11) 387. https://doi.org/10.3390/polym8110387

[23] Ashutosh, K. V., Amey, S. K., & Jindal, K. S. (2024). Estimating ionic conductivity of ionic liquids: Nernst-Einstein and Einstein formalisms. *Journal of Ionic Liquids.* Volume 4, issue 1, June 2024, 100089. https://doi.org/10.1016/j.jil.2024.100089

[24] Liew, C. W., Ramesh, S., Ramesh, K., & Arof, A. K. (2012). Preparation and characterization of lithium ion conducting ionic liquid-based biodegradable corn starch polymer electrolytes. *Journal of Solid-State Electrochemistry*. https: //doi.org/10.1007/s10008-012-1651-5

[25] Temiz, C. (2022). Scanning Electron Microscopy. *Open Access Peer-Reviewed Chapter*. https://doi.org/ 10.5772/intechopen.103956

[26] Huang, X., Leng, X., Li, T., Wang, C., Tang, T., Xie, L., Liu, B., & Zhang, S. (2024). TiO_2 inorganic nanoparticle framework enhanced PEO based solid-state electrolytes for improved performance of solid-state lithium batteries. *Research Square Platform LLC*. https://doi.org/10.21203/rs.3.rs-4136142/v1

[27] Papakyriakou, M., Lu, M., Liu, Y., Liu, Z., Chen, H., McDowell, M. T., & Xia, S. (2021). Mechanical behavior of inorganic lithium-conducting solid electrolytes. Journal of Power Sources. Volume 516, 31 December 2021, 230672. https://doi.org/10.1016/j.jpowsour.2021.230672

[28] Jing, B., Wang, X., Shi, Y., Gao, H., & Fullerton-Shirey, S. K. (2021). Combining hyperbranched and linear structures in solid polymer electrolytes to enhance structures in solid polymer electrolytes to enhance mechanical properties and room-temperature ion transport. *Frontier in Chemistry*, 9, 563864. https://doi.org/10.3389/Fchem.2021.563864

[29] Kozdra, S., Wojcik, A., Mozdzonek, M., Florczak, L., Opalinski, I. & Michalowski, P. P. (2022). Poly (vinylidene fluoride) solid polymer electrolyte structure secondary ion mass spectrometry. *Polymer*. https://doi.org/10.1016/J.polymer.2022.125364

[30] Wijanarko, N. P., Wulandari, D., Arrafii, M. H., Pradanawati, S. A., Nimah, Y. L., Noerochim, L., & Hamidah, N. L. (2024). Effect of solid polymer electrolyte based on corn starch and lanthanum nitrate on the electrochemical performance of supercapacitor. *2024, Bio Web of Conferences*, p. 03001. https://doi.org/10.1051/biocontf/20248903001